Annals of Botany **115**: 807–820, 2015
doi:10.1093/aob/mcv013, available online at www.aob.oxfordjournals.org

ANNALS OF BOTANY
Founded 1887

The *CUP-SHAPED COTYLEDON2* and *3* genes have a post-meristematic effect on *Arabidopsis thaliana* phyllotaxis

Agata Burian[1,†], Magdalena Raczyńska-Szajgin[1,†], Dorota Borowska-Wykręt[1], Agnieszka Piatek[1,‡], Mitsuhiro Aida[2] and Dorota Kwiatkowska[1,*]

[1]*Department of Biophysics and Morphogenesis of Plants, University of Silesia, Jagiellońska 28, 40-032 Katowice, Poland and* [2]*Graduate School of Biological Sciences, Nara Institute of Science and Technology, 8916-5 Takayama, Ikoma, Nara 630-0192, Japan*

* *For correspondence. E-mail dorota.kwiatkowska@us.edu.pl*

† *These authors contributed equally to this work.*

‡ *Present address: Division of Biological and Environmental Sciences and Engineering, King Abdullah University of Science and Technology, Thuwal 23955-6900, Kingdom of Saudi Arabia.*

Received: 27 October 2014 Returned for revision: 9 December 2014 Accepted: 6 January 2015 Published electronically: 12 February 2015

• **Background and Aims** The arrangement of flowers in inflorescence shoots of *Arabidopsis thaliana* represents a regular spiral Fibonacci phyllotaxis. However, in the *cuc2 cuc3* double mutant, flower pedicels are fused to the inflorescence stem, and phyllotaxis is aberrant in the mature shoot regions. This study examined the causes of this altered development, and in particular whether the mutant phenotype is a consequence of defects at the shoot apex, or whether post-meristematic events are involved.

• **Methods** The distribution of flower pedicels and vascular traces was examined in cross-sections of mature shoots; sequential replicas were used to investigate the phyllotaxis and geometry of shoot apices, and growth of the young stem surface. The expression pattern of *CUC3* was analysed by examining its promoter activity.

• **Key Results** Phyllotaxis irregularity in the *cuc2 cuc3* double mutant arises during the post-meristematic phase of shoot development. In particular, growth and cell divisions in nodes of the elongating stem are not restricted in the mutant, resulting in pedicel–stem fusion. On the other hand, phyllotaxis in the mutant shoot apex is nearly as regular as that of the wild type. Vascular phyllotaxis, generated almost simultaneously with the phyllotaxis at the apex, is also much more regular than pedicel phyllotaxis. The most apparent phenotype of the mutant apices is a higher number of contact parastichies. This phenotype is associated with increased meristem size, decreased angular width of primordia and a shorter plastochron. In addition, the appearance of a sharp and deep crease, a characteristic shape of the adaxial primordium boundary, is slightly delayed and reduced in the mutant shoot apices.

• **Conclusions** The *cuc2 cuc3* double mutant displays irregular phyllotaxis in the mature shoot but not in the shoot apex, thus showing a post-meristematic effect of the mutations on phyllotaxis. The main cause of this effect is the formation of pedicel–stem fusions, leading to an alteration of the axial positioning of flowers. Phyllotaxis based on the position of vascular flower traces suggests an additional mechanism of post-meristematic phyllotaxis alteration. Higher density of flower primordia may be involved in the post-meristematic effect on phyllotaxis, whereas delayed crease formation may be involved in the fusion phenotype. Promoter activity of *CUC3* is consistent with its post-meristematic role in phyllotaxis.

Key words: *Arabidopsis thaliana*, *cup-shaped cotyledon*, flower development, organ fusion, phyllotaxis, post-meristematic shoot development, shoot apical meristem, SAM.

INTRODUCTION

Generation of phyllotactic patterns takes place at the shoot apex when organ primordia are initiated at the periphery of the shoot apical meristem (SAM). During pattern assessment at the shoot apex or in older shoot portions, it is helpful to distinguish angular distribution and axial distribution (Williams, 1975). Angular distribution is characterized by a divergence angle measured along the ontogenetic helix that joins consecutive lateral organs or primordia, whereas axial distribution is described by internode length along the stem axis. In a number of taxa, in which lateral organs are quite closely packed even in mature shoot portions, such as needles on *Abies balsamea* Mill. twigs, contact parastichies can be used to determine the shoot phyllotaxis rather than the divergence angle (Zagórska-Marek, 1985).

Phyllotaxis of mature shoot portions is the combined effect of pattern generation at the SAM periphery and subsequent shoot growth. The latter especially affects axial distribution of the primordia, but its effect on angular distribution of organs cannot be excluded (as assumed, for example, in a theoretical model by Roberts, 1977). In general, differences in phyllotaxis between shoots can be of two types (Meicenheimer and Zagórska-Marek, 1989; Zagórska-Marek, 1994): qualitative, when angular distribution is different; or quantitative, when the angular distribution is the same but other parameters such as contact parastichy numbers and axial distribution differ.

Accordingly, the difference between phyllotaxis at the apex and in the mature portion of the same shoot is usually only quantitative.

At the earliest stages of primordium initiation, partitioning of the SAM surface takes place and the boundary between the primordium and SAM is established on the adaxial side of the primordium. This boundary region later develops into an organ axil. Formation of the boundary is accompanied by low growth rates and strong growth anisotropy, as well as reduced cell division frequency (Kwiatkowska and Dumais, 2003). Boundary regions are also characterized by a unique geometry (a saddle-like shape, a crease) and a predicted pattern of mechanical stress (Hamant *et al*., 2008; Burian *et al*., 2013). In *Arabidopsis thaliana* (L.) Heynh., *CUP-SHAPED COTYLEDON* (*CUC*) genes *CUC1*, *CUC2* and *CUC3* encoding NAC-domain transcription factors are expressed in boundary regions (Aida *et al*., 1999; Ishida *et al*., 2000; Takada *et al*., 2001; Hibara *et al*., 2006), which coincide with the region of limited cell divisions (Breuil-Broyer *et al*., 2004). Starting from embryogenesis, these transcription factors define the boundary identity (Aida and Tasaka, 2006). Single and double mutations in the *CUC* genes lead to various shoot organ fusions, to varying degrees of severity. In the *cuc2 cuc3* double mutant, flower pedicels are fused to the inflorescence stem, and phyllotaxis is aberrant in the mature shoot portions. However, how such a phenotype develops has not yet been studied. Thus, the purpose of our investigation was to identify the nature of these defects and when in the shoot development the aberrations take place. In particular, we checked whether the mutant phenotype is a consequence of defects at the shoot apex, or whether post-meristematic events are involved.

MATERIALS AND METHODS

Plant material and growth conditions

Wild type (WT) plants of *Arabidopsis thaliana* Columbia-0 (Col-0; seeds obtained from the Nottingham Arabidopsis Stock Centre, NASC) and the *cuc2-3 cuc3-105* double mutant in the Col-0 background (Hibara *et al*., 2006) were initially grown in a growth room (temperature 19–21 °C, illumination 60 μmol m^{-2} s^{-1}) under short-day conditions (9 h day/15 h night) for 3–4 weeks and then moved to a glass house with long-day conditions (14 h/10 h, temperature 20–24 °C). Plants with primary inflorescence shoots higher than 10 cm were (1) used to obtain replicas from the inflorescence shoot apices or from the young shoot surface; (2) used to prepare hand cross-sections of stems; or (3) were fixed for microtome sectioning. *pCUC3::GUS* (Kwon *et al*., 2006; a gift from Doris Wagner) were initially grown on plates under continuous white light and later on soil under long-day conditions, essentially as described previously (Takeda *et al*., 2011). Primary inflorescence shoots, approx. 15 cm high, were subjected to β-glucuronidase (GUS) staining.

Microtome sections and light microscopy

The apical parts of inflorescence shoots, 4 mm long, comprising the SAM and the young not yet fully elongated portion of the stem, were fixed in FAA (5 mL of 40 % formalin, 5 mL of glacial acetic acid, 90 mL of 50 % ethanol), dehydrated in a graded ethanol series followed by an ethanol/buthanol series, and embedded in the Paraplast Plus embedding medium (Sigma-Aldrich, No. P3683). Serial longitudinal sections, 8 μm thick, were prepared with the aid of a Leica RM 2145 microtome equipped with disposable blades (C. L. Sturkey, Inc.), mounted on glass slides, and stained by periodic acid–Schiff (PAS) reaction (Feder and O'Brien, 1968). Images were taken using a bright-field microscope (Olympus BX41) equipped with a CCD camera (Olympus XC50).

Replica method and scanning electron microscopy

Sequential replicas of the surface of shoot apices and young inflorescence shoots were obtained as described previously (Williams and Green, 1988; Kwiatkowska and Burian, 2014). Briefly, silicon polymer moulds (made of Take 1 impression material – the hydrophilic vinyl wash material, regular set, Kerr Corp., Romulus, MI, USA) were taken from the analysed surface and filled with epoxy resin (Devcon 2 ton epoxy). Epoxy resin casts were sputter-coated and observed by scanning electron microscopy (SEM; Philips XL 30 TMP ESEN). Pairs of stereoimages were obtained from each region of interest. Sequences of two replicas were taken at 24 h time intervals from 15 shoot apices of the WT, and 12 of *cuc2 cuc3*; as well as from six and five young shoot surface fragments of the WT and *cuc2 cuc3* inflorescences, respectively.

GUS staining

Visualization of GUS activity was carried out as described previously (Nahar *et al*., 2012), except that staining time was 72 h. Stained samples were post-fixed in ethanol–acetic acid solution (9:1), rehydrated and cleared in chloral hydrate–glycerol–water solution (8 g of chloral hydrate, 1 mL of glycerol and 2 mL of water).

Assessment of angular and axial flower distribution in elongated shoots

Inflorescence shoots of five WT and five *cuc2 cuc3* plants were harvested, and their basal ends submerged in a water-soluble ink for a night. The ink 'sucked' into xylem stained vascular bundles, enabling visualization of the shoot primary vasculature. Each shoot was then cross-sectioned by hand. The thickness of sections varied between 0·3 and 2·0 mm depending on the node distribution. Micrographs of side and top views of successive sections were taken under a stereomicroscope (Nikon SMZ800) using a CCD camera (Nikon DS-Fi1). The sequence of side-view micrographs obtained for each shoot was used to measure the section thickness and to assess quantitative parameters of nodes and internodes (explained further in the Results). Top-view micrographs were used to measure divergence angles in the following way. First, for each top view of the cross-section from a sequence, a few approximated diameters were drawn and their intersection was assumed to be a geometric centre of the stem. Then, the same vascular bundles

were identified in each pair of successive cross-sections (only bundles that were not related to flower traces in these stem segments were chosen); the section images were rotated and superimposed so that the positions of these bundles and stem centres nearly overlapped. After performing this operation for all the images, those images in which consecutive flower pedicels were separating from the stem were selected, and divergence angles between successive pedicels were measured with respect to the stem geometric centre (either clockwise or counterclockwise along the whole shoot, depending on its phyllotaxis). A similar procedure was performed in order to measure divergence angles between successive flower traces. The image processing was performed with the aid of CorelDRAW X6 (Corel Corp.), and measurements were made with the aid of ImageJ (National Institutes of Health; downloaded from http://rsbweb.nih.gov/ij/).

Analysis of surface area, growth and curvature

Rates of cell growth in area, surface areas and surface curvature were computed for replicas using previously described protocols (Dumais and Kwiatkowska, 2002; Routier-Kierzkowska and Kwiatkowska, 2008). Briefly, pairs of stereoimages of each region of interest were used for the stereoscopic reconstruction of the region surface. For each cell on such a reconstructed surface, maximal and minimal curvatures and their directions were computed based on the 3-D co-ordinates of vertices (three-way cell wall junctions) belonging to the cell and all its direct neighbours. Gaussian curvature was computed as the product of minimal and maximal curvatures. For each sequence of replicas, the same vertices were recognized in the consecutive replicas, and directions of maximal and minimal growth rates were first computed for each cell vertex (based on deformation of a triangle defined by the vertices that are joined with the vertex by a common cell wall). Then, the values and directions for all the cell vertices were averaged, and the areal growth rate for the cell was computed as the sum of minimal and maximal growth rates. Cell wall surface areas were computed as sums of triangles defined by 3-D co-ordinates of two cell vertices and the cell centroid. The surface area of a SAM was computed as the sum of surface areas of the outer periclinal cell walls.

All codes used for this analysis were written in Matlab (The Mathworks, Natick, MA, USA).

Assessment of phyllotaxis at shoot apices

Since SEM images of shoot apices were often not exactly the top view, which could lead to errors in divergence angle measurements, phyllotaxis was analysed in top views of shoot apex surfaces reconstructed from pairs of stereoimages (Routier-Kierzkowska and Kwiatkowska, 2008). To obtain the top view of the reconstructed apex surface, a direction normal to the SAM surface was found and the view from this direction was regarded as the top view of the apex. In such an image, outlines of the SAM and flower primordia (very young primordia were recognized by elevated Gaussian curvature at curvature maps) were digitized, and points representing the geometric centre of the meristem and the geometric centre of each visible primordium were computed. Based on these points and outlines, relative surface areas of primordia (the ratio between orthogonally projected primordium and SAM surface areas), primordium angular width (primordia of plastochron age from 3 to 6 were used for this comparison, since their boundaries are easy to define) and divergence angles between consecutive primordia were measured. Nineteen shoot apices of WT and 20 of *cuc2 cuc3* plants were analysed in this way. Additionally, for nine WT and ten mutant shoot apices, the relative surface area of primordia was used to assess the absolute surface area of these primordia on the basis of the absolute surface area of the individual SAMs. Plastochron duration was assessed on the basis of comparison of primordium size and developmental stage in two consecutive replicas of individual apices.

All codes used for this analysis were written in Matlab, and are available from the corresponding author on request.

Analysis of inner tissues of the inflorescence stems

Using the longitudinal microtome sections of young shoot fragments, surface areas of an axil cortex region and of cortex cells included in this region were measured at each node, with the aid of ImageJ. An axil cortex region was defined as a section fragment delimited by the epidermis, stem vascular bundles and the flower trace diverging at this node. Surface area was measured for all the cortex cells visible in this section fragment. Sections of eight stems with 3–7 nodes each were analysed both for the WT and *cuc2 cuc3*, which in total gives 40 nodes with 15–40 cells each for the WT, and 41 nodes with 15–250 cells each for the mutant plants.

Statistics

For each set of data, the Kolmogorov–Smirnoff test was used to check if data distribution is normal. For samples with normal distribution or samples with >100 measurements, the *t*-test was used for pair-wise comparisons of differences between sample means; other samples were compared using Mann–Whitney test (Zar, 1999). Statistical tests and graphic illustration were obtained with the aid of Origin 8.6.0 (OriginLab Corp., Northampton, MA, USA) or Matlab Statistics Toolbox.

RESULTS

Phyllotactic patterning is impaired in elongated parts of cuc2 cuc3 *inflorescence shoots*

The most striking feature of the elongated parts of the *cuc2 cuc3* shoots is the fusion of the inflorescence stem and basal portions of pedicels, resulting in a fasciated-like appearance (Fig. 1A, B). To check whether this defective organ separation is accompanied by defects in angular distribution of flowers (siliques) around the inflorescence stem, we first assessed the divergence angle between pedicels in elongated stem portions, further referred to as the pedicel phyllotaxis. It was performed by measuring angles between consecutive pedicels at levels where they become separated (depart) from the stem, in series of stem cross-sections. In all the five WT shoots examined, we observed a regular spiral Fibonacci phyllotaxis (Fig. 1C), with a mean divergence angle of 135·94° [standard deviation

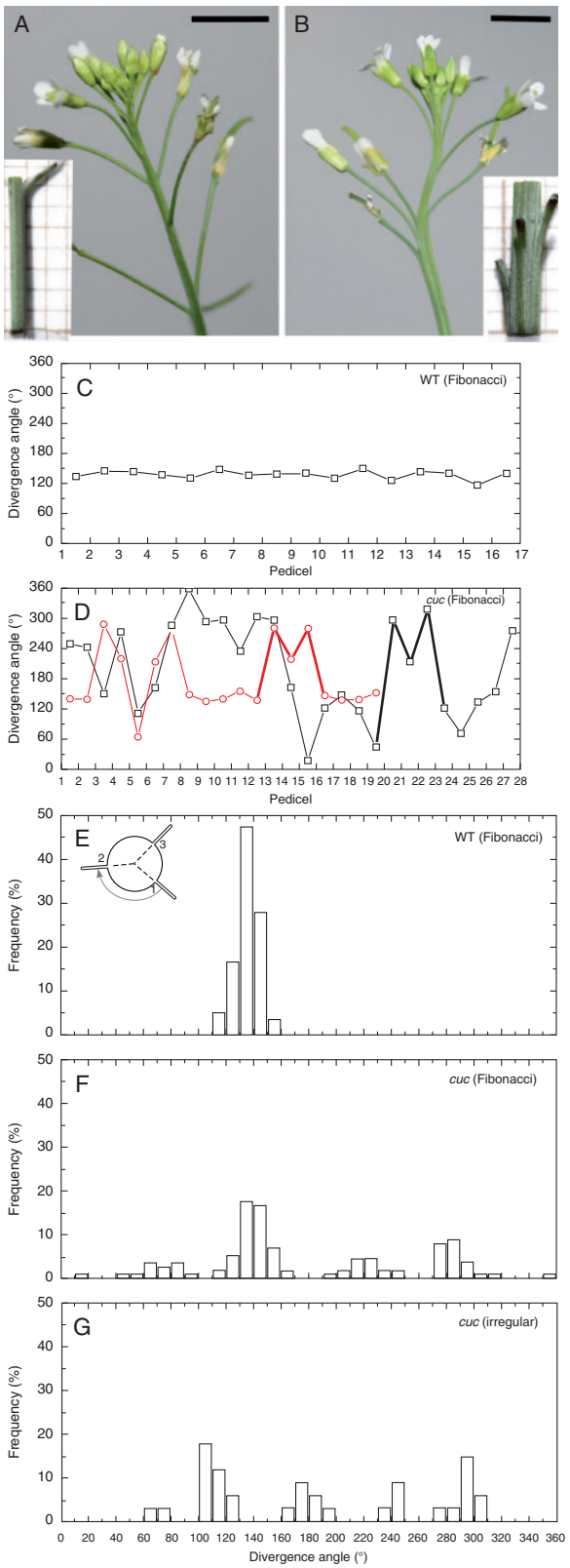

FIG. 1. Pedicel phyllotaxis. Inflorescence shoots of WT (A) and *cuc2 cuc3* (B) plants. Insets show magnified views of elongated shoot fragments with one (A) or several (B) pedicels departing from the stem (the background grid is 1 × 1 mm). Note the uneven distribution of pedicels along the stem, and fusions between the stem and pedicels in the mutant. Scale bars = 5 mm. (C, D) Graphs representing the divergence angle measured between consecutive pedicels of one exemplary WT (C) and two *cuc2 cuc3* (D) shoots, indicated by different colours. Line segments representing exemplary M-motifs (D) are thickened. (E–G) Histograms of divergence angles measured between pedicels at levels where they separate from the stem for WT (E) and *cuc2 cuc3* (F, G) plants.

(s.d.) = 8·89 °; median = 136·88 °]. Among the five *cuc2 cuc3* mutant shoots analysed, four exhibited the spiral Fibonacci phyllotaxis in apical portions, and one displayed an irregular flower arrangement. In these four mutant shoots, the divergence angle was nevertheless significantly higher (*t*-test; $P = 0{\cdot}05$) and more variable (mean = 176·41 °; s.d. = 74·05 °; median = 147·81 °) than that of the WT (compare graphs in Fig. 1D and C). A histogram of angles pooled for the WT shoots with Fibonacci phyllotaxis shows a unimodal distribution (Fig. 1E; 61 angles for five shoots), whereas that of the mutant Fibonacci shoots was multimodal (Fig. 1F; 115 angles for four shoots). In both cases, the highest peak was at 130–140 °. On the other hand, no dominating peak was apparent in the histogram for the mutant shoot with an irregular pedicel arrangement (Fig.1G). Thus, defective organ separation in the *cuc2 cuc3* mutant is accompanied by less regular organ positioning around the stem in its elongated portion.

To explain this relationship we examined the axial distribution of flowers along the stem and analysed more closely the fusions between pedicels and the stem in series of stem cross-sections. For each pedicel we first identified the level where a vascular bundle supplying this pedicel (flower trace) leaves the vascular cylinder of the stem (level a), and the level at which the pedicel becomes separated from the stem (level c) (Fig. 2A–D). In the WT, the distance between levels a and c was short and relatively uniform along an individual stem (Fig. 2B, E) while in *cuc2 cuc3* it was much larger and variable (Fig. 2D, E). Moreover, closer inspection of mutant stems allowed us to distinguish an additional level (level b), which is never encountered in the WT. This level is located between the levels a and c and is marked by the appearance of a stripe of chlorenchyma that extends towards level c forming a connection (fusion) between the stem and the pedicel (Fig. 2C). Apparently, variation in the distances between these three levels, especially between levels b and c (Fig. 2D, E), could explain some of the defects in mutant pedicel phyllotaxis. In particular, if we assume that the order of organ production is manifested by the position of the flower trace, it appears that older pedicels were sometimes separated later from the stem than younger ones (e.g. in Fig. 2D older pedicels 9 and 10 are separated from the stem at 25–30 mm from the apex, but younger pedicels 11 and 12 are separated at 40 mm from the apex). This resulted in a locally reversed order of pedicels in the sequence used for divergence angle measurements in pedicel phyllotaxis.

Next we checked whether pedicel–stem fusions are accompanied by altered internode length of inflorescence stems. We assumed that the internode length is a distance between levels at which successive flower traces leave the stem vascular cylinder (i.e. the distance between level a of consecutive flowers, ordered on the basis of their flower trace positions). Comparison of mean distances (Fig. 2F) showed that in the WT they are significantly larger (mean = 8·75 mm; s.d. = 4·31 mm;

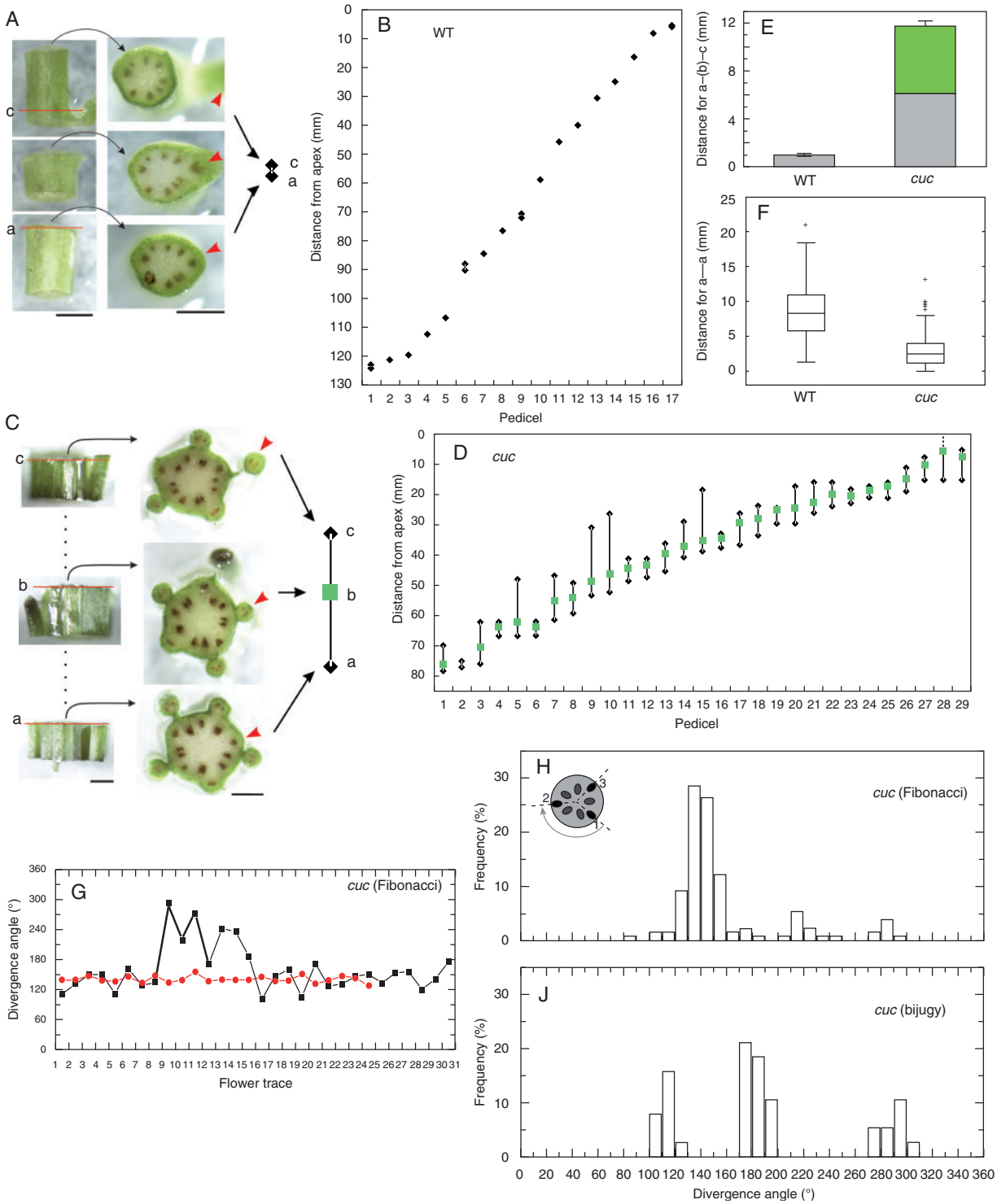

FIG. 2. Axial distribution of pedicels and flower traces, and vascular phyllotaxis. (A–F) Axial distribution. Fragments of WT (A) and *cuc2 cuc3* (C) shoots and their sections, as those used for distribution assessments of pedicels or flower vascular traces. Levels a, b and c are marked by red line segments in side views of sections. In the WT shoot, the distance from level a to c is 0·78 mm; in the mutant it is 7·08 mm from level a to b, and 5·70 mm from b to c. Scale bars = 0·5 mm. (B and D) Distances from the shoot apex to levels a and c of each flower in an exemplary WT shoot (B), or from the apex to levels a, b and c for a *cuc2 cuc3* shoot (D). (E) Distance between levels a and c in WT and *cuc2 cuc3* shoots (mean ± s.e.m.). In the mutant, the green bar portion represents distances between levels b and c, i.e. the segment with chlorenchyma. (F) Distances between levels a of consecutive flowers in WT and *cuc2 cuc3* shoots. A solid line within each box represents the median. The box delimits the first and third quantiles. Whiskers extend from each end of the box to the adjacent values in the data as long as the most extreme values are within 1·5 times the interquartile range from the ends of the box. Crosses represent outliers, i.e. data with values beyond the ends of the whiskers. (G) Graphs representing the divergence angle measured between consecutive vascular traces of two *cuc2 cuc3* shoots, the same as in Fig. 1D, where they are marked with the same colours as here. The black-labelled shoot is also the same one as that shown in (D). Line segments representing an exemplary M-motif are thickened. (H and J) Histograms of divergence angles in vascular phyllotaxis, i.e. measured between levels a of successive flowers in *cuc2 cuc3* shoots with different phyllotaxis.

median = 8·35 mm) than in *cuc2 cuc3* (mean = 2·87 mm; s.d. = 2·23 mm; median = 2·32 mm) plants (*t*-test; $P = 0{\cdot}05$). We conclude that the fusions may reduce stem/internode elongation.

Mutant phyllotaxis assessed on the basis of flower vascular traces is more regular than pedicel phyllotaxis

For the assessment of the pedicel phyllotaxis, we used the divergence angles between the level at which pedicels depart from the stem (levels c). Since the extent of pedicel fusion in *cuc2 cuc3* affects the order of this class of levels and thus the pedicel phyllotaxis, we next examined the angular distribution of flower traces in the same shoots (vascular phyllotaxis), by measuring the divergence angles between consecutive flower traces at level a.

In the WT we assumed that the divergence angles in vascular and pedicel phyllotaxis are the same, because levels a and c are very close. In *cuc2 cuc3* stems with the Fibonacci pattern, vascular phyllotaxis was much more regular than in the pedicel phyllotaxis (compare graphs of the same colours in Figs 1D and 2G, and histograms in Figs 1F and 2H). Although it was less regular than in the WT (compare Figs 1E and 2H) and the histogram for the mutant vascular phyllotaxis is still multimodal, the peak at 130–140 ° is much higher than others. Moreover, the mean divergence angle and the variation of divergence angle for the mutant vascular phyllotaxis (mean = 157·18 °; s.d. = 42·24 °; median = 142·70 °) are much lower than the mutant pedicel phyllotaxis (mean = 176·41 °; s.d. = 74·05 °; median = 147·81 °). Closer inspection showed that in only a few cases in the mutant was the order of flower traces reversed with respect to that expected from the spiral Fibonacci pattern (black graph in Fig. 2G), as manifested in angle value peaks at 280–290 and 210–220 ° in Fig. 2H (Besnard *et al*., 2014).

We also examined divergence angles of the flower traces for the mutant shoot with irregular pedicel phyllotaxis (Fig. 2J). In cross-sections of this stem it was apparent that there were pairs of opposite flower traces (angular distance of 180 °). Although they did not leave the vascular cylinder at the same level, the mean distance between the traces in each pair was significantly shorter than that between the traces of consecutive pairs (1·7 mm vs. 2·8 mm; *t*-test, $P = 0{\cdot}05$). On the other hand, in the distribution of angles for this shoot there are three peaks: the highest at 170–180 °, and two lower peaks at 110–120 and 290–300 °; and the frequency for the angle range 170–200 ° is approx. 50 % (Fig. 2J). Such a distribution can be interpreted as resembling the bijugate spiral phyllotaxis (Fig. 2J), in which a pair of opposite organs is formed at each node and the relative position of adjacent pairs is not symmetrical, resulting in the two remaining peaks.

In summary, the phyllotactic pattern based on vascular traces is generally more regular than that of pedicels in *cuc2 cuc3* mutant inflorescences. Clearly then, the observed irregularity in the pedicel phyllotaxis of the mutant shoots is related to the fusions between pedicels and stem.

As the *CUC2* and *CUC3* genes have been shown to be expressed in the boundary regions between primordia and the SAM (Hibara *et al*., 2006), we expected that the organ fusion and resulting phyllotactic defects might already be visible in the primordium arrangement around the SAM. We thus analysed the phyllotactic pattern at the inflorescence shoot apex.

Phyllotaxis is regular at cuc2 cuc3 *shoot apices*

In order to characterize phyllotaxis at shoot apices of *cuc2 cuc3* plants, we first measured divergence angles between consecutive flower primordia (Fig. 3A, B). Surprisingly, we did not find any alterations of phyllotaxis in the mutant. Rather, a regular spiral Fibonacci pattern was characteristic for both WT and mutant apices, with the mean divergence angle of 143·34 ° (s.d. = 9·50 °) for the WT and 143·65 ° (s.d. = 9·62 °) for the mutant. We also found a single case of a Lucas spiral pattern (with the divergence angle approx. 90 °; excluded from Fig. 3B) among 20 examined apices of *cuc2 cuc3*.

Nevertheless, comparison of other phyllotaxis parameters (Fig. 3C–M) showed differences between *cuc2 cuc3* and WT plants. First, the numbers of contact parastichies in the mutant are higher than in the WT (Fig. 3C). In particular, families of three, five and eight parastichies are apparent in most mutant apices (Fig. 3H–K) while in the WT, families of three and five parastichies are dominant (Fig. 3F, G). Secondly, the angular width of primordia is lower in *cuc2 cuc3* than in the WT (mean = 73·8 ° and s.d. = 8·1 ° in the WT; mean = 69·0 ° and s.d. = 8·7 ° in the mutant; statistically significant difference, *t*-test, $P = 0{\cdot}05$). Thirdly, the surface area of the mutant SAM is increased (Fig. 3D; statistically significant difference; Mann–Whitney test, $P = 0{\cdot}05$), while the surface areas of the younger primordia in the mutant are initially similar to those of the WT and decreased in consecutive plastochrons (Fig. 3E; differences for pair-wise comparisons between primordia of the same plastochron age are statistically significant for primordia 3 and 4 but not for 1 and 2; Mann–Whitney test, $P = 0{\cdot}05$). Moreover, comparison of primordia in two consecutive replicas of individual apices (Fig. 3L, M) shows that the plastochron duration is decreased in the mutant. In the WT apex (Fig. 3L), for example, primordium 2 at time 24 h attains a developmental stage between the stages of primordium 3 and 4 at time 0 h, which means that more than one but less than two plastochrons have passed during the 24 h (approx. 1·5 plastochrons per 24 h). In the case of the mutant apex (Fig. 3M), primordium 1 at time 24 h attains a developmental stage equivalent to that of primordium 3 at time 0 h, which means that two plastochrons have passed during the 24 h. All these differences show that in the mutant, flower primordia are more closely packed around the SAM than those in the WT, are initiated at an increased rate and are smaller with respect to the SAM. In addition, it cannot be excluded that some primordia are formed almost simultaneously in the mutant apices with high contact parastichy numbers (compare, for example, the youngest primordia in the apex shown in Fig. 3K), suggesting a slight disturbance in the order of primordium formation.

On the basis of these observations, we conclude that the defects in phyllotactic patterning that we observe in the mature stem portions of *cuc2 cuc3* plants are mainly the effect of the mutations on post-meristematic development. In order to check whether there is any meristematic trait that could possibly be amplified in the course of post-meristematic development and

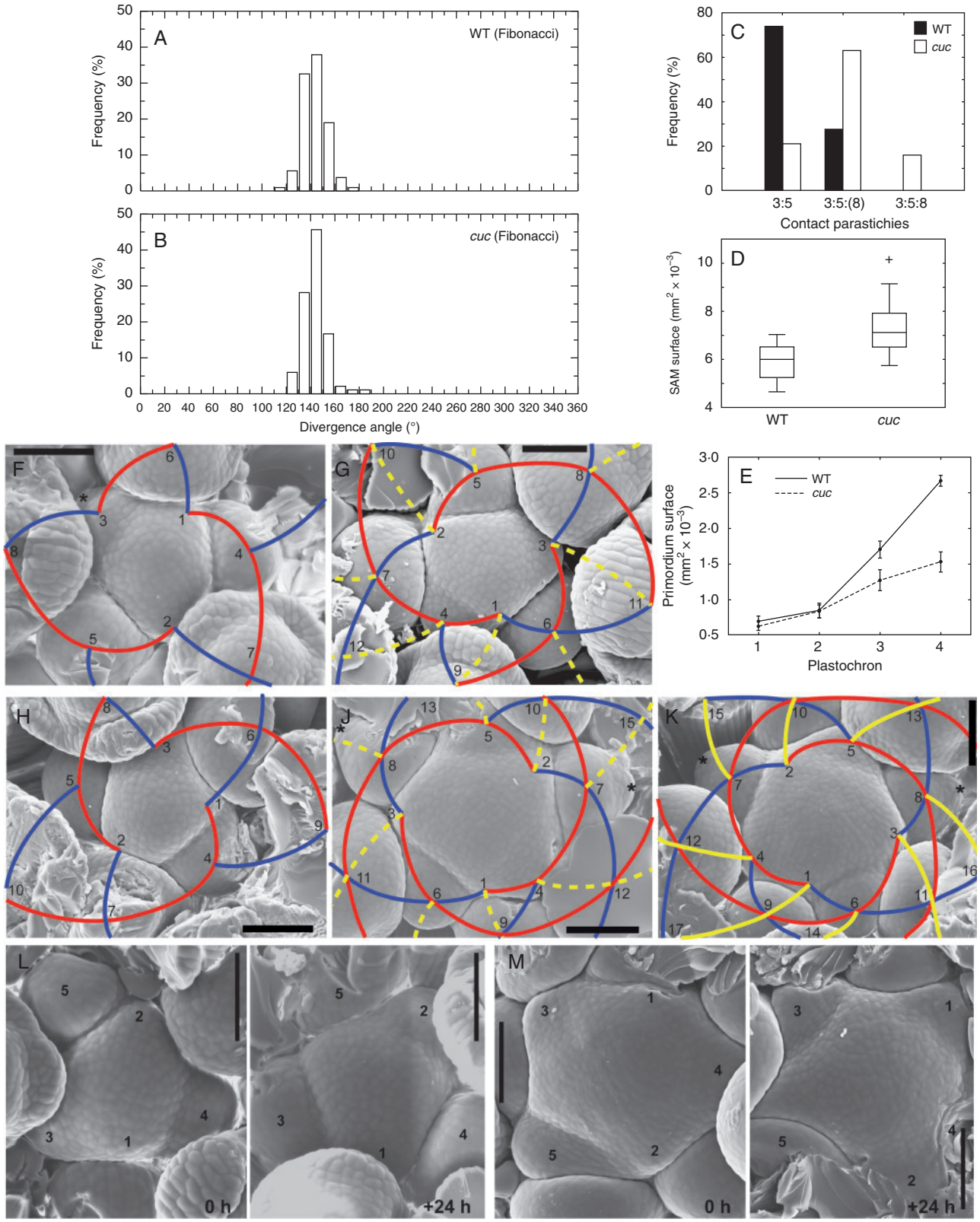

FIG. 3. Phyllotaxis at inflorescence shoot apices. (A and B) Histograms of divergence angles in WT (A) and *cuc2 cuc3* (B) shoot apices. (C) Frequency of different contact parastichy numbers in the WT and *cuc2 cuc3*. (D) Surface areas of SAMs in the WT and *cuc2 cuc3*. Boxplots are as in Fig. 2F. (E) Surface areas of primordia of different plastochron age (mean ± s.e.m.) in the WT and *cuc2 cuc3*. (F–K) Contact parastichies drawn on SEM micrographs for exemplary apices of the WT (F and G) and *cuc2 cuc3* (H–K). Families of three parastichies are drawn in red, five in blue and eight in yellow. Less apparent parastichies are in dashed lines. Asterisks label rudimentary bracts. Flower primordia are numbered according to their plastochron age. (L and M) Consecutive replicas of WT (L) and *cuc2 cuc3* (M) shoot apices taken at a 24 h time interval. Flower primordia are numbered according to their plastochron age at time 0 h in order to facilitate comparison between the two replicas. Scale bars = 100 µm.

TABLE 1. *Duration of early flower developmental stages*

Line	Plastochron age of primordium		
	Bulging at the initial crease	The oldest primordium with rudimentary bract	The youngest primordium with lateral sepals
WT	$3{\cdot}30^{a} \pm 0{\cdot}47$ (23)	$4{\cdot}89^{a} \pm 0{\cdot}78$ (9)	$6{\cdot}74^{a} \pm 0{\cdot}54$ (21)
cuc2 cuc3	$3{\cdot}79^{b} \pm 0{\cdot}71$ (19)	$6{\cdot}27^{b} \pm 1{\cdot}27$ (11)	$8{\cdot}71^{b} \pm 1{\cdot}51$ (14)

Values are means ± s.d. with the number of apices sampled given in parentheses

Different indices refer to statistically significant differences for pair-wise comparisons in columns (Mann–Whitney test, $P = 0{\cdot}05$).

could lead to phyllotaxis defects in the mutant, we examined in more detail the geometry of the shoot apex, especially the boundary region between the primordium and SAM, as well as node/internode development of the inflorescence stems.

Duration of early stages of primordium development is affected by cuc2 cuc3 *mutations*

We first examined the plastochron age of primordia exhibiting the early developmental stages, i.e. bulging at the initial crease, the disappearance of rudimentary bract and the appearance of lateral sepals (Table 1; Kwiatkowska, 2006; Alvarez-Buylla *et al*., 2010). Comparison between *cuc2 cuc3* and WT apices shows that all the stages appear at later plastochron in the mutant plants. These differences most probably result mainly from the decreased plastochron duration, while the differences in absolute time may be insignificant. However, the apparent effect of the mutations is the extended persistence of rudimentary bracts: in the WT, the rudimentary bracts are apparent for less than one plastochron (Kwiatkowska, 2006) while they persist for at least two plastochrons in the mutant apices (compare Fig. 3F with 3J and K; Fig. 4C).

Next we examined the formation of the boundary between the SAM and flower primordium (adaxial primordium boundary) in the mutant and WT. In both genotypes, the boundary region between the SAM and flower primordium is saddle-shaped, i.e. convex in the latitudinal direction (along the SAM circumference) and concave in the meridional direction (across the boundary; Fig. 4). Since in the mutant the boundaries seem to be less distinct (compare primordium 5 boundary in Fig. 3G and J), we compared the minimal values of Gaussian curvature at the bottom of the boundary assigned to primordia of the same plastochron age, and showed that the mean curvature values are indeed lower in the WT, i.e. the 'sharper' boundary is formed earlier than in the mutant (Table 2). Next, in order to discriminate between the direct effect of the mutations and the effect of differences in plastochron duration and primordia packing, we carefully selected WT apices to be compared with the mutant, so that both the primordia packing and the developmental stage of the youngest flower primordia are similar. A detailed analysis of the apex geometry confirmed a slight delay in the boundary formation in the mutant if primordia of a similar plastochron age are compared (compare primordia 5 in Fig. 4). Also, the boundary between older primordia and the SAM in the mutant is less prominent than in the WT (compare Fig. 4E and F).

Thus, we propose that defects in phyllotactic patterning in elongated stem portions due to fusions between the pedicels and the stem may be to a certain extent explained by a slight delay and reduction of boundary formation at the mutant shoot apex. To examine this in more detail, we focused on node and internode development in the sub-apical stem portion and its elongation zone.

Cell growth and divisions are not inhibited near the site of pedicel attachment to the cuc2 cuc3 *stem*

Stem organization into nodes and internodes is evident in elongating and mature portions of stems in many species, where the two types of regions are alternating stem segments. Identification of nodes and internodes, however, is much less obvious in younger stem portions, especially in the case of shoots with spiral phyllotaxis and dense packing of primordia. In such cases, one can apply the stem unit, i.e. a stem portion comprising the site of primordium attachment and the portion below, delineated by planes including fragments of contact parastichies and stem axis as well as the primordium axil (Meicenheimer, 1992, 2006). During shoot development, growth of stem units is such that each unit gives rise to a single node and a subtending internode.

Using the sequential replicas, we quantified epidermal cell growth and divisions on the surface of young stems and pedicel bases of WT and mutant plants, up to 5 mm from the shoot apex (Fig. 5). In the young stem portions, where the stem unit notion is applicable, only the region adjacent to the pedicel–stem junction, not the whole stem disk at the node level, is expected to exhibit reduced growth and cell division frequency. Indeed, in the WT stem portion close to the apex, the rate of both areal growth and cell division is lower in the regions near the pedicel–stem junction than that in adjacent regions including the surface of the stem (Fig. 5A) and this pattern is maintained in the lower (more mature) stem portion (Fig. 5C). The mutant displays a growth and cell division pattern similar to the WT in the portion close to the apex (compare Fig. 5A, B), but a strong effect was observed in the lower stem portion (compare Fig. 5C, D). In this portion, a fusion between stem and pedicels becomes apparent, and in regions near pedicel–stem junctions, epidermal cells keep on growing and dividing unlike in the WT stems. In this stem portion in the WT, nodes and internodes can already be distinguished, while due to stem–pedicel fusions they are virtually indistinguishable in the mutant.

Next, we examined inner stem tissues at pedicel–stem junctions in longitudinal sections of mutant and WT stems. To this end, we first defined the axil cortex region, to be delimited by the vascular bundles of the stem and the flower trace that diverges at the node (outlined in Fig. 5E, F). We then compared the mean surface area of cells in the axil cortex regions at different distances from the apex (Fig. 5G) and showed that these cortical cells are larger in the mutant than in the WT. In particular, in the mutant the mean cell surface area increases rapidly with the distance from the apex, till about 0·4 mm from the apex. In the WT, mean cell area increases more slowly and at 0·2 mm cells attain an almost maximal size, which is much smaller than in the mutant.

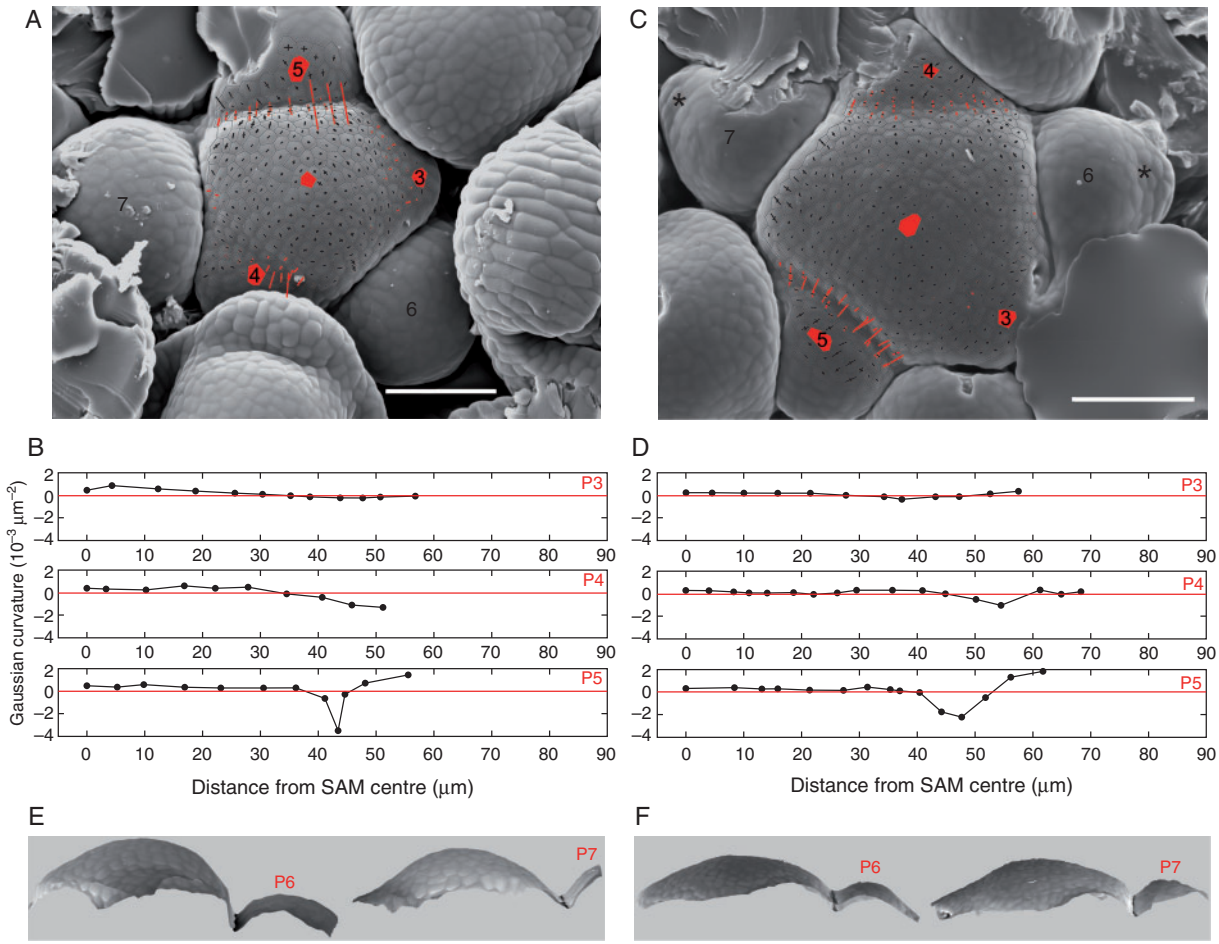

FIG. 4. Shoot apex geometry in the WT (A, B, E) and *cuc2 cuc3* (C, D, F). (A and C) Cell outlines are overlaid on SEM micrographs. Crosses represent maximal and minimal curvatures; cross arms are proportional to curvature values and appear in black if the apex surface in this direction is convex, or in red if it is concave. Cells located at the SAM and primordia centres are labelled with red. Black asterisks label rudimentary bracts. Scale bars = 100 µm. (B and D) Gaussian curvature at centres of cells located along line segments between the SAM centre and primordium centre, plotted against the distance from the SAM centre. The same primordia numbers are used in Gaussian curvature plots and SEM micrographs. (E and F) Side views of the reconstructed surface of WT (E) and mutant (F) apices shown in (A) and (C), respectively. Two views of each apex are presented, visualizing profiles of creases between the SAM and primordia 6 and 7.

TABLE 2. *Shoot apex geometry at the adaxial primordium boundary*

Line	Minimal Gaussian curvature at primordium 4 or 5 boundary in 10^{-3} µm^{-2}	
	P4	P5
WT	$-1{\cdot}44^{a} \pm 0{\cdot}69$ (12)	$-2{\cdot}97^{a} \pm 1{\cdot}19$ (3)
cuc2 cuc3	$-0{\cdot}66^{b} \pm 0{\cdot}56$ (11)	$-1{\cdot}08^{b} \pm 1{\cdot}05$ (11)

Values are means ± s.d. with the number of apices sampled given in parentheses

Different indices refer to statistically significant differences for pair-wise comparisons in columns (Mann–Whitney test, $P = 0{\cdot}05$).

We also compared the surface area of the axil cortex regions in the mutant and the WT, using the longitudinal shoot sections (Fig. 5H). In agreement with the shoot surface observations, there was only a slight difference between the WT and the mutant plants in apical parts of the stem (up to approx. 0·2 mm from the apex). Further from the apex the area of the axil region in the WT was no longer increasing, while in the mutant it continuously increased. Since the size of cortex cells in the mutant increased up to 0·4 mm from the apex and was constant at larger distance from the apex (Fig. 5G), the further increase of axil region area implies that cell divisions must have taken place. Therefore, we conclude that the formation of the tissue at the fusion between the pedicel and stem in *cuc2 cuc3* resulted from both cell expansion and cell divisions at the axil cortex region.

In summary, the phenotype of the *cuc2 cuc3* mutant, i.e. defective phyllotaxis of the elongated shoot portions, is a consequence of not only a slight delay in the boundary formation at the shoot apex, but also of the aberrant pattern of stem elongation in post-meristematic development.

Expression pattern of CUC3 *suggests a direct post-meristematic effect of mutation*

Since the analysis of stem growth further confirmed the post-meristematic effect of the mutations, we checked the spatial

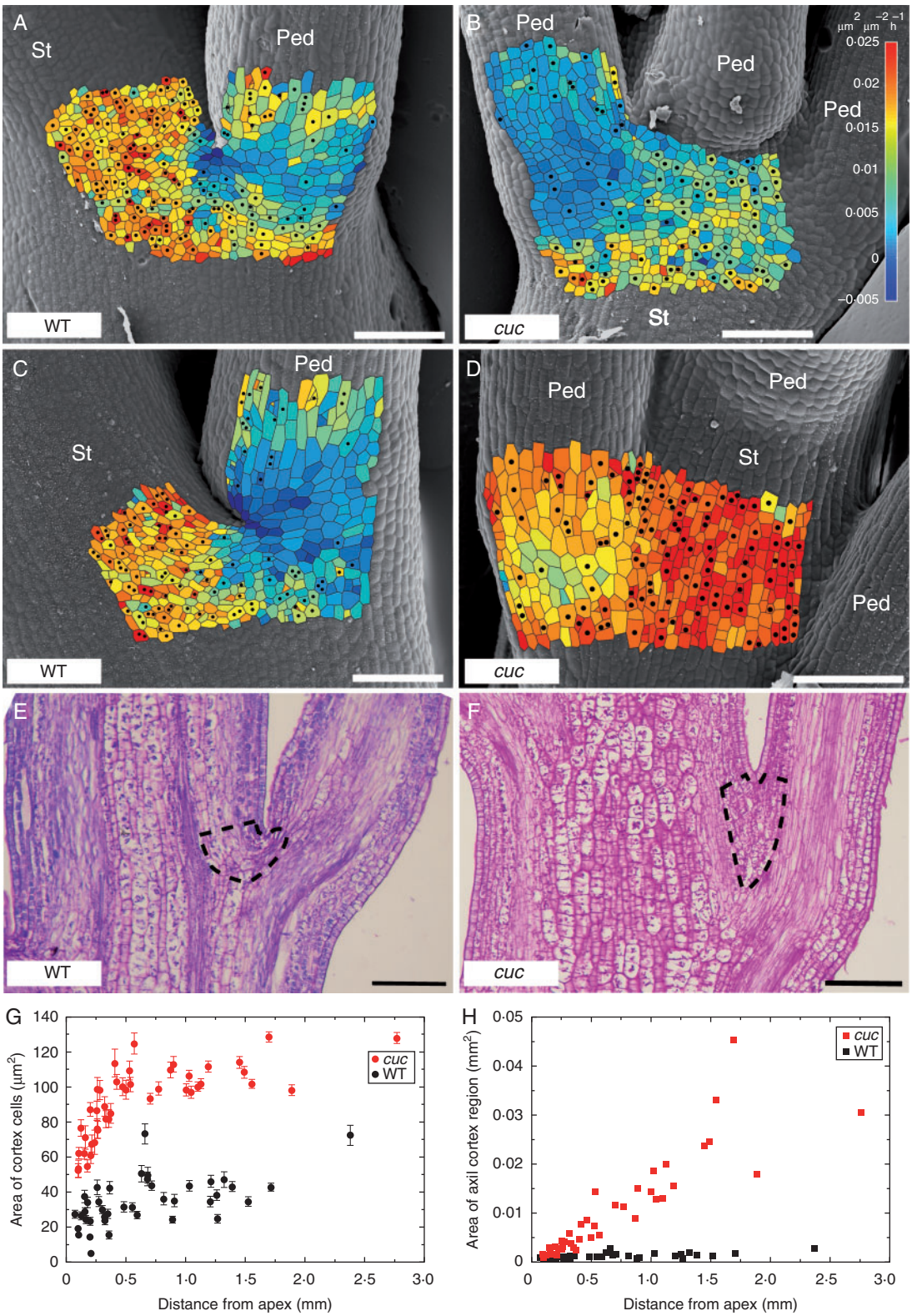

FIG. 5. Growth and cell divisions in young stems. (A–D) SEM micrographs of the shoot surface in the WT (A, C) and *cuc2 cuc3* (B, D). Shoot fragments are <1 mm (A, B) or approx. 3 mm (C, D) from the shoot apex. Colour maps representing growth rates in area of cells are overlaid on the SEM micrographs; dots label cells that divide during the next 24 h. The micrographs are from replicas taken at the beginning of the 24 h interval for which the growth rates were computed. Stem (St) and pedicels (Ped) are labelled. (E and F) Fragments of longitudinal sections of WT (E) and *cuc2 cuc3* (F) shoots, approx. 2 mm from the shoot apex. Axil cortex regions are outlined. Scale bars = 100 μm. (G and H) Surface area of cortex cells (G; mean ± s.e.m.) and of axil cortex regions (H) in WT (black) and *cuc2 cuc3* (red) shoots, plotted against the distance from the shoot apex, for axil regions of all the shoots analysed.

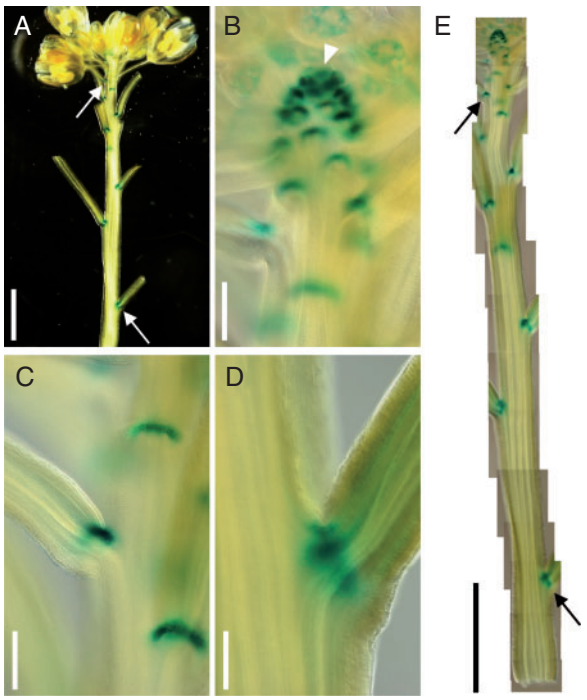

FIG. 6. Whole-mount GUS staining of the *pCUC3::GUS* inflorescence shoot. (A) Whole view. Upper and lower arrows indicate the positions corresponding to (C) and (D), respectively. (B–D) Close-up images at the shoot apex (B) and at the positions approx. 1·2 mm (C) and approx. 10 mm (D) below the apex of the shoot shown in (A). (E) Combined image of a photographic series taken along the shoot shown in (A). Arrows in (A) and (E) indicate the positions that correspond to (C) and (D). The arrowhead in (B) indicates the SAM. Scale bars = 2 mm in (A) and (E); and 200 µm in (B–D).

and temporal expression patterns of *CUC2* and *CUC3* in WT shoots. Peaucelle *et al*. (2007) showed that *CUC2* expression is not limited to the shoot apex but is also detected later during shoot development, in axils of flower pedicels. Thus we checked the expression pattern of *CUC3* using the *pCUC3::GUS* reporter (Kwon *et al*., 2006; Fig. 6). The pattern of *CUC3* expression in the inflorescence shoot is very similar to that of *CUC2*. Not only at the shoot apex but also in the elongating and even at mature portions of inflorescence shoot, strong reporter activity is present in pedicel axils, i.e. at the adaxial portion of the junction between the pedicel and inflorescence stem. Thus, the expression patterns of *CUC2* and *CUC3* further support the post-meristematic roles for these genes in maintaining regular phyllotaxis.

DISCUSSION

At macroscopic examination, inflorescence shoot phyllotaxis of the *cuc2 cuc3* double mutant appears irregular. Using methods facilitating the comparison of the arrangement of vascular flower traces and pedicels in the same shoots, we show that this irregularity arises mainly during the post-meristematic phase of shoot development, especially in the course of stem elongation when growth and cell divisions at nodes are not restricted, while the arrangement of flower primordia at the mutant shoot apex is nearly as regular as in the WT. The regularity of the arrangement of the flower primordium in the mutant is accompanied by the regularity of vascular phyllotaxis, known to be generated at the shoot apex almost simultaneously with the phyllotactic pattern (Dengler, 2006).

The main difference between the shoot apices of *cuc2 cuc3* and of the WT is the increased density of primordia around the mutant SAM, which is related to the increased SAM surface area in the mutant. This phenotype is manifested by higher numbers of contact parastichies and by a lower relative size of primordia. We also demonstrated a slight delay in the appearance of the crease, which is a characteristic shape of the adaxial flower primordium boundary, and reduction of its depth.

Phyllotaxis aberrations in cuc2 cuc3 *mature inflorescence shoot portions and their origin*

The most apparent effect of the *cuc2 cuc3* mutations on inflorescence shoot morphology are aberrant phyllotaxis and fusions between flower pedicels and the stem. These two traits are related. Since the distance along the fused region of the pedicels and stem is quite variable, a pedicel of a flower predicted to be produced earlier (the first on an ascending ontogenetic helix) often departs from the stem at the level higher than that of the next flower, i.e. their order along the helix is reversed. The fusions themselves may thus explain some reversions in the axial distribution of pedicels, and thus the observed phyllotaxis alterations in the mutant. Consistently, angular distribution of vascular flower traces, whose final positioning is much less affected by pedicel fusions, is much more regular compared with that of pedicels. Nevertheless, we also observed much less evident, but significant, irregularity in the angular distribution of vascular flower traces in contrast to regular phyllotaxis in the shoot apex, indicating an additional cause for post-meristematic phyllotaxis alterations, possibly related to nearly simultaneous formation of some primordia. Local reversions of axial organ distribution are not uncommon in shoots of plants with spiral phyllotaxis and densely packed leaves, for example *Abies balsamea* (see, for example, needle arrangement in the shoot shown in fig. 6A of Zagórska-Marek, 1985). The occurrence of reversions, referred to as permutations of organ insertion order, has also been reported for plants with less dense organ packing, such as *Helianthus annuus* L. (Couder, 1998) and *A. thaliana* WTs and mutants (Guédon *et al*., 2013; Besnard *et al*., 2014). Theoretical models show that such permutations can be an intrinsic trait of spiral phyllotaxis (Mirabet *et al*., 2012; Guédon *et al*., 2013). A so-called M-shaped motif in divergence angle plots is a manifestation of permutations. In the mutant of the *ARABIDOPSIS HISTIDINE PHOSPHOTRANSFER PROTEIN 6* gene in which cytokinin signalling is affected, the increased frequency of permutations is related to the presence of pairs or triplets of flower primordia exhibiting virtually the same developmental stage (Besnard *et al*., 2014). In *cuc2 cuc3*, the comparison of the arrangement of the vascular flower traces and the pedicels in the same shoots shows that the M-shaped motif occurs both in pedicel and, less often, in vascular phyllotaxis as manifested in divergence angle plots (Figs 1D and 2G) and histograms, which are multi- instead of unimodal (with additional peaks at approx. 220 and 280 °). Since the vascular phyllotaxis is generated at the shoot apex almost simultaneously with the phyllotactic pattern (Dengler, 2006), some

reversions (permutations) presumably appear early in shoot development. Moreover, in the case of shoot apices with higher contact parastichy numbers, the difference in the developmental stage of consecutive primordia along the ontogenetic spiral are smaller than in the case of less densely packed primordia (compare, for example, differences between primordia 2–4 in Fig. 3H, J). Judging from the occurrence of reversions in species such as *A. balsamea*, one may expect that the reversions are more likely when primordia packing at the apex is denser. This is also confirmed by the comparison between *A. thaliana* plants grown in various day-length conditions showing that in plants with larger SAMs and denser packing of primordia the frequency of permutations (reversions) is higher (Landrein *et al*., 2014). The denser primordia packing in *cuc2 cuc3* plants may thus be another reason for aberrant phyllotaxis in mature portions of mutant shoots, making the reversion of pedicel separation and of flower traces order at the elongated stem more probable.

Strong expression of both *CUC2* and *CUC3* is characteristic of boundaries between the inflorescence SAM and primordia. However, despite the phyllotaxis aberrations in mature shoot portions of the *cuc2 cuc3* mutant plants, phyllotaxis at the inflorescence shoot apex in the mutant is virtually as regular as that in the WT. Similarly, plants expressing a microRNA-resistant *CUC2* gene show regular primordium arrangement at the shoot apex but a strongly altered arrangement of pedicels on fully grown shoots (Peaucelle *et al*., 2007). In this case, ectopic expression of *CUC2* in the internode is associated with the changes in cell number and cell size, resulting in abnormal internode lengths. A similar phenotype is also observed in the triple mutant of the three *mir164* genes, which negatively regulate CUC1 and CUC2 (Sieber *et al*., 2007). Together, these results indicate that the activities of *CUC1*, *CUC2* and *CUC3* do not affect angular positioning of flower primordia at the shoot apex but affect post-meristematic shoot development, in particular the process of node/internode formation.

Pedicel–stem fusions and formation of nodes and internodes in cuc2 cuc3 *mutant stems*

We show that formation of pedicels fused with stems in the *cuc2 cuc3* shoots is accompanied by unrestricted growth and cell divisions in the stem regions that correspond to both future nodes and internodes in the WT. This phenotype is apparent only at some distance from the shoot apex where internodes start to elongate. This observation, together with the expression pattern of *CUC2* and *CUC3* in elongating portions of *A. thaliana* inflorescence shoots, suggests that fusion formation is the direct effect of the mutations on post-meristematic growth.

The occurrence of pedicel–stem fusions is accompanied by shortening of mutant internodes. Phytohormones are known to be a major factor regulating stem elongation (e.g. Sachs, 1965; Yamaguchi and Komeda, 2013). In *cuc2 cuc3*, however, the observed internode shortening seems rather to be a secondary effect of fusions. In WT *A. thaliana*, elongation of an internode lasts longer than that of the pedicels attached at its base (Yamaguchi and Komeda, 2013). The difference in potential elongation capacity between the internodes and pedicels quite probably leads to restriction of internode elongation in the mutant. Since the stem is most often surrounded by fused pedicels, this restriction usually does not lead to stem bending as would be the case if a single pedicel were fused with the stem.

Effects of cuc2 cuc3 *on the inflorescence shoot apex*

An unexpected effect of the *cuc2 cuc3* mutations is the increased density of primordia packing around the SAM. The mutant shoot apex also shows enlarged SAM size and shorter plastochrons. The shorter plastochrons most probably result in increased duration of early stages of flower primordium development measured in terms of the number of plastochrons. However, slower progression of mutant primordium development in the real time scale cannot be excluded. In other species, such as *Linum usitatissimum* L. (Williams, 1975) and spruce *Picea abies* (L.) Karst. (Gregory and Romberger, 1972), the numbers of contact parastichies at the apex are known to increase spontaneously during shoot apex ontogeny. This increase takes place without any change in primordium identity or initial size but is accompanied by a decrease in plastochron duration and increase in the SAM size, as well as a resulting decrease in relative primordium size. These differences are similar to those between *cuc2 cuc3* and WT apices. Such relationships between primordia packing, SAM size and primordium size have also been shown in phyllotaxis models (e.g. Meicenheimer and Zagórka-Marek, 1989; Douady and Couder, 1996).

A change in primordia packing around the SAM may be induced by phytohormone treatment or mutations. Although the former most often leads to a change in divergence angles, in some cases, such as *Xanthium pennsylvanicum* Wallr. vegetative shoot apices, application of gibberellin (GA_3 in lanolin paste) results in an increase of contact parastichy numbers and the size of SAM with no effect on the divergence angle (Maksymowych and Erickson, 1977). Mutations in the *ABERRANT PHYLLOTAXY1* (*ABPHYL1*) gene of *Zea mays* L. lead to an increase of primordia number per node in whorled phyllotaxis accompanied by an increase in the SAM size (decussate phyllotaxis appears in place of distichous phyllotaxis in the mutant; Greyson *et al*., 1978), which is analogous to the increase in density of primordia packing. *ABPHYL1* regulates *PIN-FORMED1* (*PIN1*) expression, affecting the auxin level at the SAM, and cytokinin-induced expansion of the SAM (Giulini *et al*., 2004; Lee *et al*., 2009). An increase in primordia packing in spiral phyllotaxis, originally described as increased spiral parastichy winding, is caused by mutations in the *BELLRINGER* (*BLR*) gene (Byrne *et al*., 2003). *BLR* encodes a transcription factor interacting with STM, known to regulate cytokinin synthesis and repress auxin response in regulating the SAM function (Murray *et al*., 2012). Also Landsberg *erecta A. thaliana* plants exhibit denser primordia packing than other ecotypes, such as Col-0 or Wassilewskija (D. Kwiatkowska and A. Burian, unpubl. res.). It is noteworthy that the ERECTA family of receptor-like kinases regulate the SAM size and interact with auxin transport or sensitivity to cytokinins (Van Zanten *et al*., 2009; Shpak, 2013; Uchida *et al*., 2013). It may thus be expected that the observed effect of the *cuc2 cuc3* mutations on primordia packing is also due to interaction with phytohormone-related processes. Indeed, CUC1 and CUC2

transcription factors have already been shown to affect PIN1 expression and polarity, thus altering auxin distribution in processes related to leaf and carpel margin shape formation (Bilsborough *et al*., 2011; Galbiati *et al*., 2013).

The *cuc2 cuc3* mutations affect to some extent the SAM surface partitioning, i.e. formation of the boundary between primordium and the SAM where both genes are specifically and strongly expressed. Judging from the phenotype of the mature shoot portion of *cuc2 cuc3* plants, one would expect quite serious problems with boundary formation at the mutant shoot apex that would result in altered apex geometry in these special regions. However, the only difference in the shoot apex geometry between the mutant and WT that we were able to detect by comparing mutant with WT apices representing the same contact parastichy numbers is a slight delay in formation of a sharp crease between the primordium and the SAM, and reduction of its depth. It may thus be supposed that *CUC2* and *CUC3* are not the only factors that are sufficient to define the SAM–primordium boundary.

Conclusions

The observed phenotype of the mature inflorescence shoot in the *cuc2 cuc3* double mutant seems to result from combination of a number of effects: a slight delay in crease formation at the adaxial flower primordium boundary and increased density of primordia packing around the SAM; and later during shoot development (in the elongation zone), unrestricted growth and cell divisions within the whole stem units. The fusions between pedicels and the stem are the direct effect of the mutations, but the slight delay of crease formation amplified during post-meristematic development as well as increased primordia packing at the mutant apex, that possibly makes reversions of primordia more likely, may also be involved.

ACKNOWLEDGEMENTS

We thank Dr Ewa Teper (Laboratory of Scanning Electron Microscopy, Faculty of Earth Sciences, University of Silesia) for her excellent technical assistance with scanning electron microscopy, and Dr Sarah Robinson (University of Bern, Switzerland) for her help in correcting the final version of this manuscript. A.B. was supported by a Scholarship for Outstanding Young Scientists from the Polish Minister of Science and Higher Education.

LITERATURE CITED

Aida M, Tasaka M. 2006. Morphogenesis and patterning at the organ boundaries in the higher plant shoot apex. *Plant Molecular Biology* **60**: 915–928.

Aida M, Ishida T, Tasaka M. 1999. Shoot apical meristem and cotyledon formation during *Arabidopsis* embryogenesis: interaction among the *CUP-SHAPED COTYLEDON* and *SHOOT MERISTEMLESS* genes. *Development* **126**: 1563–1570.

Alvarez-Buylla ER, Benítez M, Corvera-Poiré A, *et al.* 2010. Flower development. *The Arabidopsis Book* **8**: e0127.

Besnard F, Refahi Y, Morin V, *et al.* 2014. Cytokinin signalling inhibitory fields provide robustness to phyllotaxis. *Nature* **505**: 417–421.

Bilsborough GD, Runions A, Barkoulas M, *et al.* 2011. Model for the regulation of *Arabidopsis thaliana* leaf margin development. *Proceedings of the National Academy of Sciences, USA* **108**: 3424–3429.

Breuil-Broyer S, Morel P, de Almeida-Engler J, Coustham V, Negrutiu I, Trehin C. 2004. High-resolution boundary analysis during *Arabidopsis thaliana* flower development. *The Plant Journal* **38**: 182–192.

Burian A, Ludynia M, Uyttewaal M, *et al.* 2013. A correlative microscopy approach relates microtubule behaviour, local organ geometry, and cell growth at the *Arabidopsis* shoot apical meristem. *Journal of Experimental Botany* **64**: 5753–5767.

Byrne ME, Groover AT, Fontana JR, Martienssen RA. 2003. Phyllotactic pattern and stem cell fate are determined by the *Arabidopsis* homeobox gene *BELLRINGER*. *Development* **130**: 3941–3950.

Couder Y. 1998. Initial transitions, order and disorder in phyllotactic patterns: the ontogeny of *Helianthus annuus*. A case study. *Acta Societatic Botanicorum Poloniae* **67**: 129–150.

Dengler NG. 2006. The shoot apical meristem and development of vascular architecture. *Canadian Journal of Botany* **84**: 1660–1671.

Douady S, Couder Y. 1996. Phyllotaxis as a dynamical self organizing process. III: The simulation of the transient regimes of ontogeny. *Journal of Theoretical Biology* **178**: 295–312.

Dumais J, Kwiatkowska D. 2002. Analysis of surface growth in shoot apices. *The Plant Journal* **31**: 229–241.

Feder N, O'Brien TP. 1968. Plant microtechnique: some principles and new methods. *American Journal of Botany* **55**: 123–142.

Galbiati F, Sinha Roy D, Simonini S, *et al.* 2013. An integrative model of the control of ovule primordia formation. *The Plant Journal* **76**: 446–455.

Giulini A, Wang J, Jackson D. 2004. Control of phyllotaxy by the cytokinin-inducible response regulator homologue *ABPHYL1*. *Nature* **430**: 1031–1034.

Gregory RA, Romberger JA. 1972. The shoot apical ontogeny of the *Picea abies* seedling. I. Anatomy, apical dome diameter, and plastochron duration. *American Journal of Botany* **59**: 587–597.

Greyson RI, Walden DB, Hume JA. 1978. The ABPHYL syndrome in *Zea mays*. II. Patterns of leaf initiation and the shape of the shoot meristem. *Canadian Journal of Botany* **56**: 1545–1550.

Guédon Y, Refahi Y, Besnard F, Farcot E, Godin Ch, Vernoux T. 2013. Pattern identification and characterization reveal permutations of organs as a key genetically controlled property of post-meristematic phyllotaxis. *Journal of Theoretical Biology* **338**: 94–110.

Hamant O, Heisler MG, Jönsson H, *et al.* 2008. Developmental pattering by mechanical signals in *Arabidopsis*. *Science* **322**: 1650–1655.

Hibara K, Karim Md R, Takada S, *et al.* 2006. *Arabidopsis CUP-SHAPED COTYLEDON3* regulates postembryonic shoot meristem and organ boundary formation. *The Plant Cell* **18**: 2946–2957.

Ishida T, Aida M, Takada S, Tasaka M. 2000. Involvement of *CUP-SHAPED COTYLEDON* genes in gynoecium and ovule development in *Arabidopsis thaliana*. *Plant and Cell Physiology* **41**: 60–67.

Kwiatkowska D. 2006. Flower primordium formation at the *Arabidopsis* shoot apex: quantitative analysis of surface geometry and growth. *Journal of Experimental Botany* **57**: 571–580.

Kwiatkowska D, Burian A. 2014. Sequential replicas for *in vivo* imaging of growing organ surfaces. In: V Žárský, F Cvrčková, eds. *Plant cell morphogenesis: methods and protocols*. New York: Springer, 99–110.

Kwiatkowska D, Dumais J. 2003. Growth and morphogenesis at the vegetative shoot apex of *Anagallis arvensis* L. *Journal of Experimental Botany* **54**: 1585–1595.

Kwon CS, Hibara K, Pfluger J, *et al.* 2006. A role for chromatin remodeling in regulation of CUC gene expression in the *Arabidopsis* cotyledon boundary. *Development* **133**: 3223–3230.

Landrein B, Refahi Y, Besnard F, *et al.* 2014. Meristem size contributes to the robustness of phyllotaxis in *Arabidopsis*. *Journal of Experimental Botany* (in press).

Lee B, Johnston R, Yang Y, *et al.* 2009. Studies of *aberrant phyllotaxy1* mutants of maize indicate complex interactions between auxin and cytokinin signaling in the shoot apical meristem. *Plant Physiology* **150**: 205–216.

Maksymowych R, Erickson RO. 1977. Phyllotactic change induced by gibberellic acid in *Xanthium* shoot apices. *American Journal of Botany* **64**: 33–44.

Meicenheimer RD. 1992. Cellular basis for growth and tissue differentiation patterns in *Linum usitatissimum* (Linaceae) stems: the stem unit. *American Journal of Botany* **79**: 914–920.

Meicenheimer RD. 2006. Stem unit growth analysis of *Linum usitatissimum* (Linaceae) internode development. *American Journal of Botany* **93**: 55–63.

Meicenheimer RD, Zagórska-Marek B. 1989. Consideration of the geometry of the phyllotaxic triangular unit and discontinuous phyllotactic transitions. *Journal of Theoretical Biology* **139**: 359–368.

Mirabet V, Besnard F, Vernoux T, Boudaoud A. 2012. Noise and robustness in phyllotaxis. *PLoS Computational Biology* **8**: e1002389

Murray JAH, Jones A, Godin Ch, Traas J. 2012. Systems analysis of shoot apical meristem growth and development: integrating hormonal and mechanical signaling. *The Plant Cell* **24**: 3907–3919.

Nahar Most. A-U, Ishida T, Smyth DR, Tasaka M, Aida M. 2012. Interactions of *CUP-SHAPED COTYLEDON* and *SPATULA* genes control carpel margin development in *Arabidopsis thaliana*. *Plant and Cell Physiology* **53**: 1134–1143.

Peaucelle A, Morin H, Traas J, Laufs P. 2007. Plants expressing a *miR164*-resistant *CUC2* gene reveal the importance of post-meristematic maintenance of phyllotaxy in *Arabidopsis*. *Development* **134**: 1045–1050.

Roberts DW. 1977. A contact pressure model for semi-decussate and related phyllotaxis. *Journal of Theoretical Biology* **68**: 583–597.

Routier-Kierzkowska A-L, Kwiatkowska D. 2008. New stereoscopic reconstruction protocol for scanning electron microscope images and its application to *in vivo* replicas of the shoot apical meristem. *Functional Plant Biology* **35**: 1034–1046.

Sachs RM. 1965. Stem elongation. *Annual Review of Plant Physiology* **16**: 73–96.

Shpak ED. 2013. Diverse roles of *ERECTA* family genes in plant development. *Journal of Integrative Plant Biology* **55**: 1238–1250.

Sieber P, Wellmer F, Gheyselinck J, Riechmann JL, Meyerowitz EM. 2007. Redundancy and specialization among plant microRNAs: role of the *MIR164* family in developmental robustness. *Development* **134**: 1051–1060.

Takada S, Hibara K, Ishida T, Tasaka M. 2001. The *CUP-SHAPED COTYLEDON1* gene of *Arabidopsis* regulates shoot apical meristem formation. *Development* **128**: 1127–1135.

Takeda S, Hanano K, Kariya A, *et al.* 2011. CUP-SHAPED COTYLEDON1 transcription factor activates the expression of *LSH4* and *LSH3*, two members of the ALOG gene family, in shoot organ boundary cells. *The Plant Journal* **66**: 1066–1077.

Uchida N, Shimada M, Tasaka M. 2013. *ERECTA*-family receptor kinases regulate stem cell homeostasis via buffering its cytokinin responsiveness in the shoot apical meristem. *Plant and Cell Physiology* **54**: 343–351.

Van Zanten M, Snoek B, Proveniers MCG, Peeters AJM. 2009. The many functions of ERECTA. *Trends in Plant Science* **14**: 214–218.

Williams MH, Green PB. 1988. Sequential scanning electron microscopy of a growing plant meristem. *Protoplasma* **147**: 77–79.

Williams RF. 1975. *The shoot apex and leaf growth*. New York: Cambridge University Press.

Yamaguchi N, Komeda Y. 2013. The role of *CORYMBOSA1*/*BIG* and auxin in the growth of *Arabidopsis* pedicel and internode. *Plant Science* **209**: 64–74.

Zagórska-Marek B. 1985. Phyllotactic patterns and transitions in *Abies balsamea*. *Canadian Journal of Botany* **63**: 1844–1854.

Zagórska-Marek B. 1994. Phyllotaxic diversity in *Magnolia* flowers. *Acta Societatis Botanicorum Poloniae* **63**: 117–137.

Zar JH. 1999. *Biostatistical analysis*. New Jersey: Prentice-Hall Inc.